Electronic Supplementary Material (ESI) for Physical Chemistry Chemical Physics.

Supporting information

Maxime Grasser,[a] and Boris Le Guennic*[a]

[a]Univ Rennes, CNRS, ISCR (Institut des Sciences Chimiques de Rennes) UMR 6226, F-35000 Rennes, France. E-mail: boris.leguennic@univ-rennes.fr

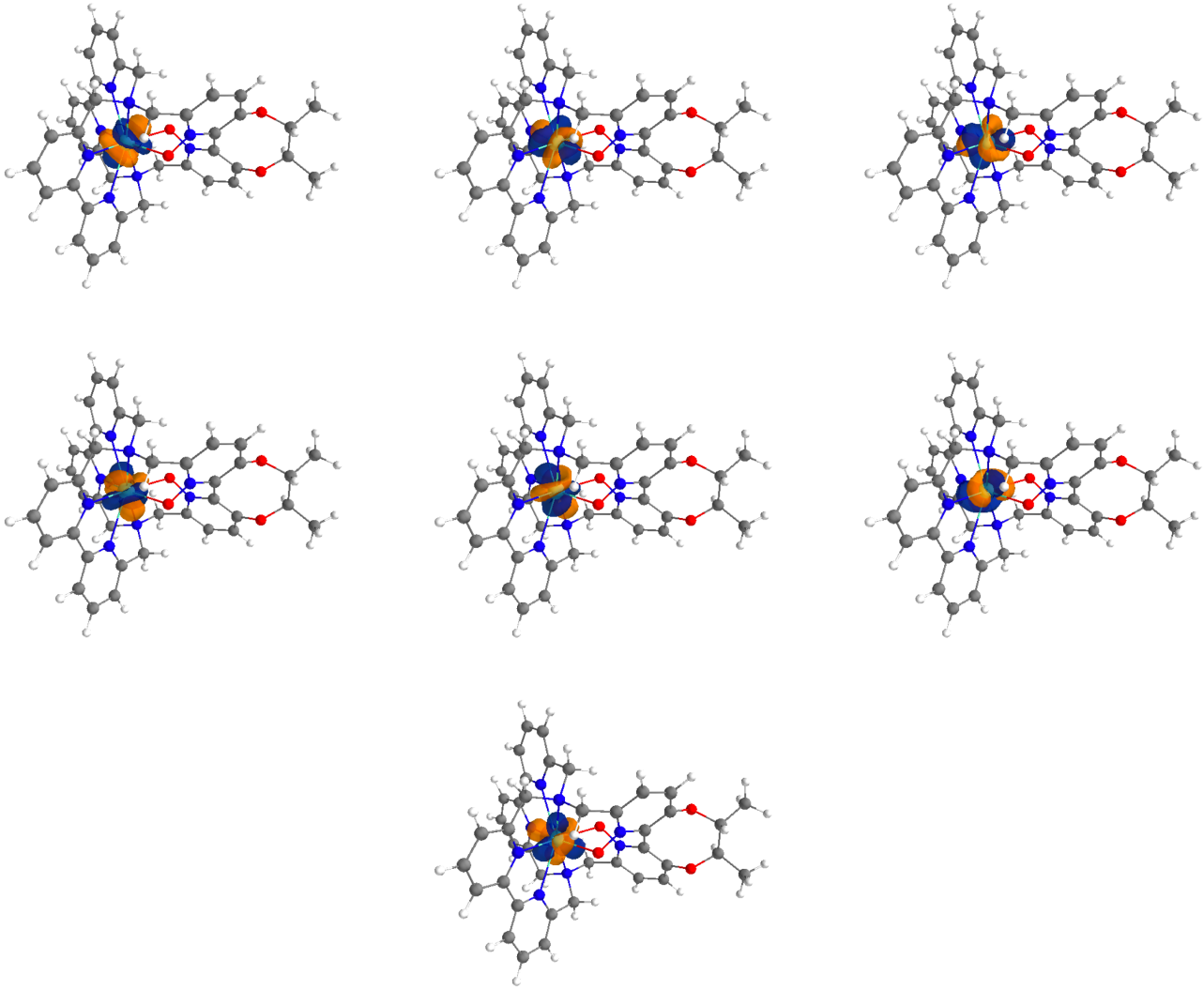

Figure S1 Plot of the isosurfaces ($\pm$0.03 au) of the 4f state-averaged natural orbitals obtained at SA-CAS(5,7)SCF/RASSI-SO level of theory for $[Sm^{III}(cryptate)]^{3+}$ complex.

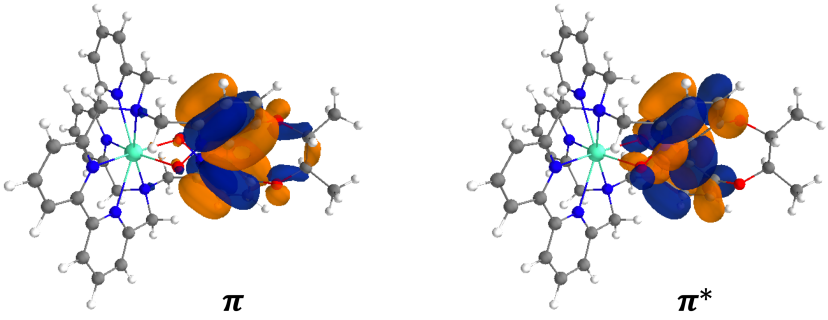

Figure S2 Plot of the isosurfaces (±0.03 au) of the π and π^* state-averaged natural orbitals involved in the SA-RAS[7,1,1,1,7,1]SCF/RASSI-SO calculations for $[Sm^{III}(cryptate)]^{3+}$ complex.

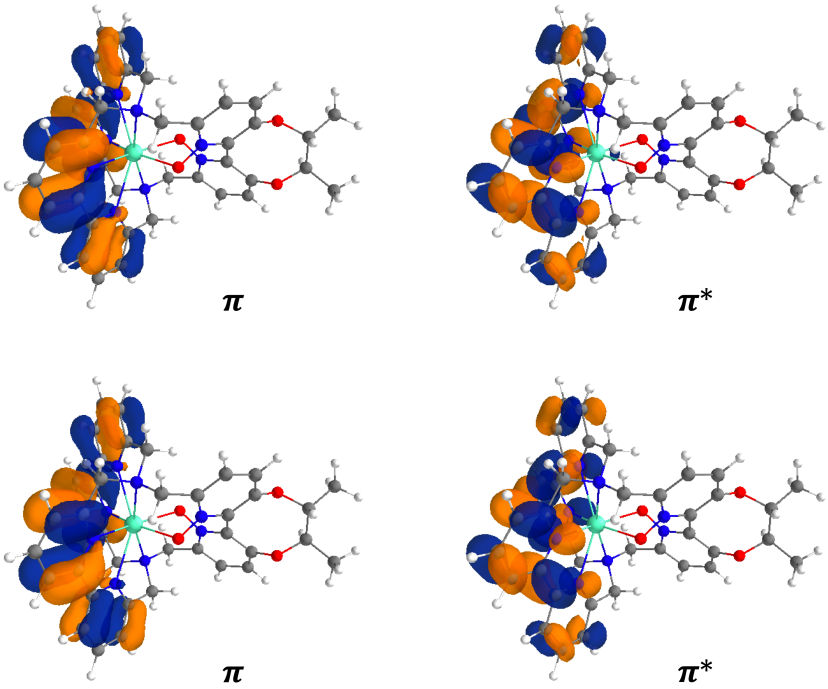

Figure S3 Plot of the isosurfaces (±0.03 au) of the π and π^* state-averaged natural orbitals involved in the SA-RAS[9,1,1,2,7,2]SCF/RASSI-SO calculations for $[Sm^{III}(cryptate)]^{3+}$ complex.

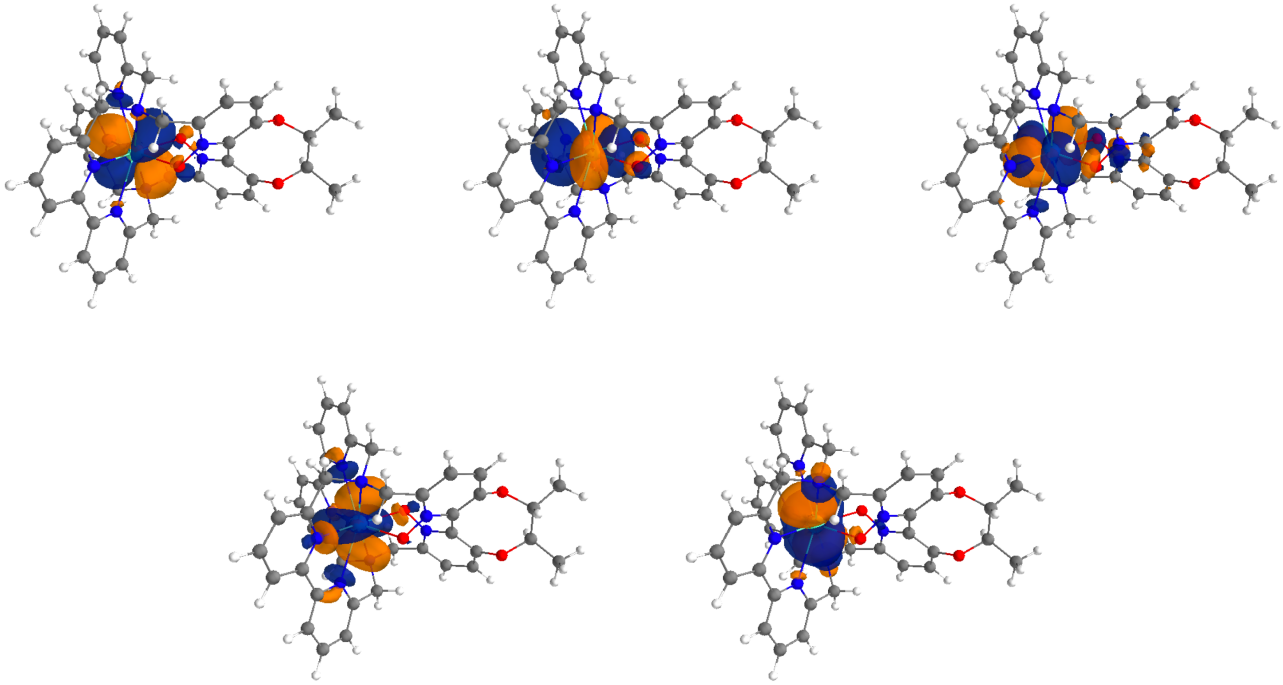

Figure S4 Plot of the isosurfaces ($\pm$0.03 au) of the 5*d* state-averaged natural orbitals involved in the SA-RAS[5,0,1,0,7,5]SCF/RASSI-SO calculations for $[Sm^{III}(cryptate)]^{3+}$ complex.

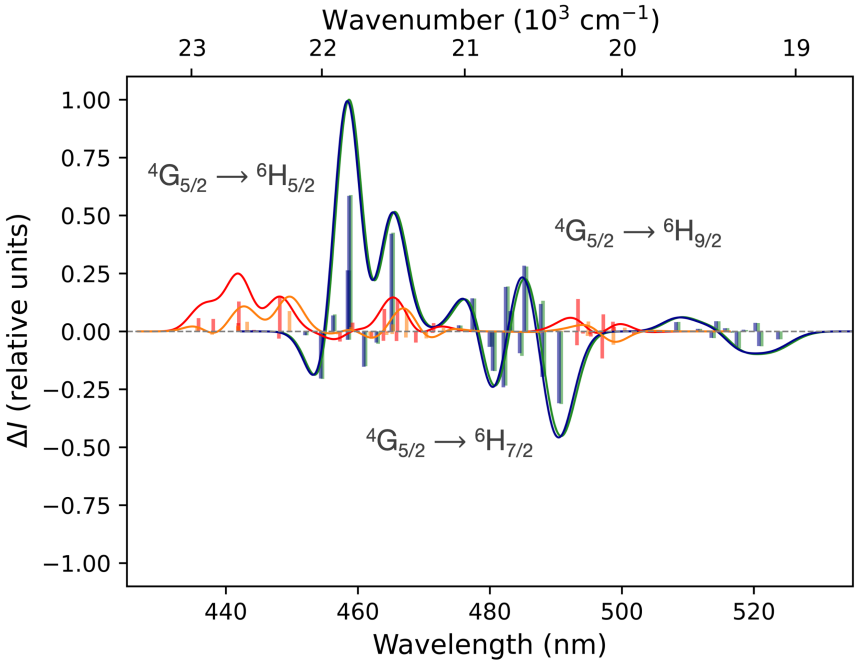

Figure S5 Simulated CPL spectra of $[Sm^{III}(cryptate)]^{3+}$ with various number of CSFs for each spin multiplicity: RASSI 1 (orange) RASSI 2 (red) RASSI 3 (blue) RASSI 4 (green). Calculations were done at SA-CAS(5,7)SCF/RASSI-SO level of theory. Calculated rotatory strengths indicated as "stick" spectra. No energetic shift has been applied.

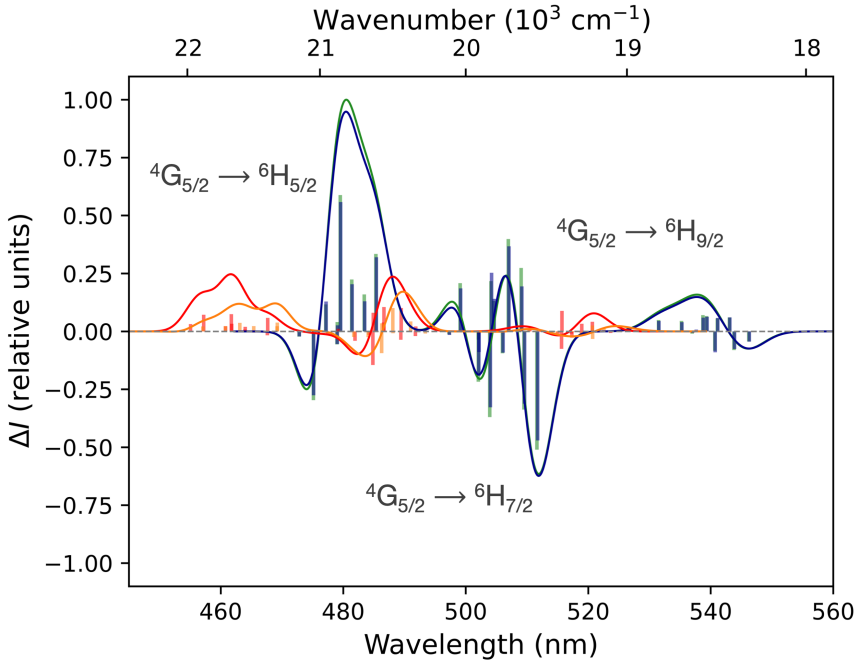

Figure S6 Simulated CPL spectra of $[Sm^{III}(cryptate)]^{3+}$ with various numbers of CSFs for each spin multiplicity: 18, 48, 0 (orange) 32, 119, 32 (red) 39, 146, 130 (blue) 103, 229, 279 (green) for sextet, quartet and doublet, respectively. Calculations were done at the SA-RAS[7,1,1,1,7,1]SCF/RASSI-SO level of theory with the 7 $4f$ orbitals of Sm in RAS2 and 1 π and 1 π^* orbital of the tether in RAS1 and RAS3, respectively. Calculated rotatory strengths indicated as "stick" spectra. No energetic shift has been applied.

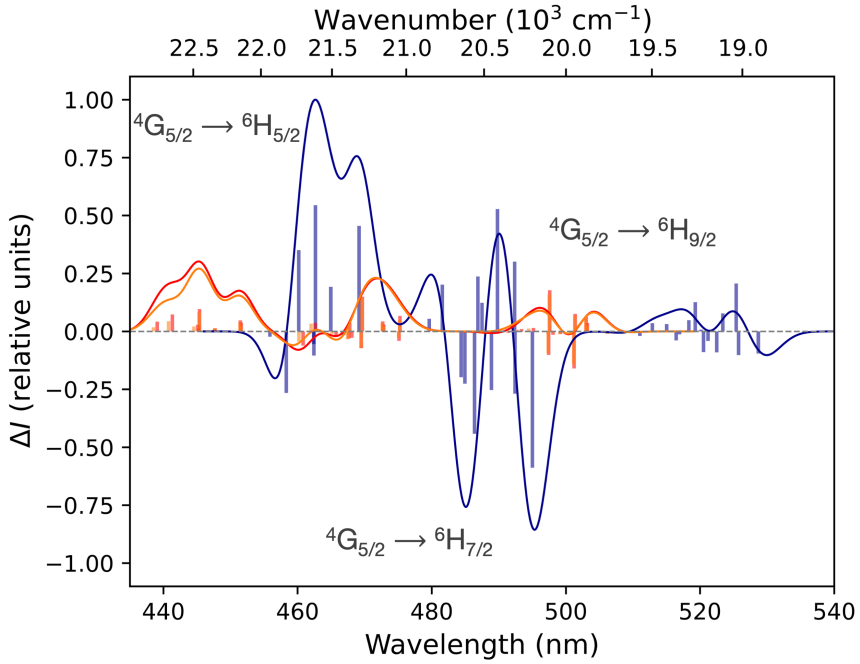

Figure S7 Simulated CPL spectra of $[Sm^{III}(cryptate)]^{3+}$ with various numbers of CSFs for each spin multiplicity: 43, 130, 0 (orange) 43, 130, 32 (red) 57, 164, 92 (blue) for sextet, quartet and doublet respectively. Calculations were done at the SA-RAS[9,1,1,2,7,2]SCF/RASSI-SO level of theory with the 7 $4f$ orbitals of Sm in RAS2 and 2 π and 2 π^* orbitals of bipyridine units in RAS1 and RAS3 respectively. Calculated rotatory strengths indicated as "stick" spectra. No energetic shift has been applied.

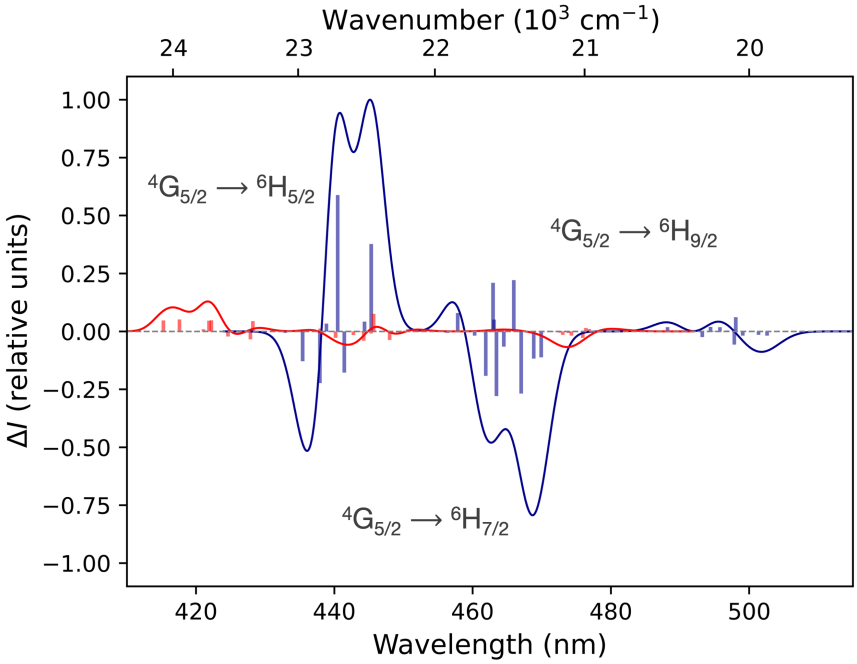

Figure S8 Simulated CPL spectra of $[Sm^{III}(cryptate)]^{3+}$ with various numbers of CSFs for each spin multiplicity: 43, 108, 32 (red) 139, 440, 419 (blue) for sextet, quartet and doublet, respectively. Calculations were done at the SA-RAS[5,0,1,0,7,5]SCF/RASSI-SO level of theory with the 7 $4f$ orbitals in RAS2 and 5 $5d$ orbitals in RAS3 of Sm(III). Calculated rotatory strengths indicated as "stick" spectra. No energetic shift has been applied.

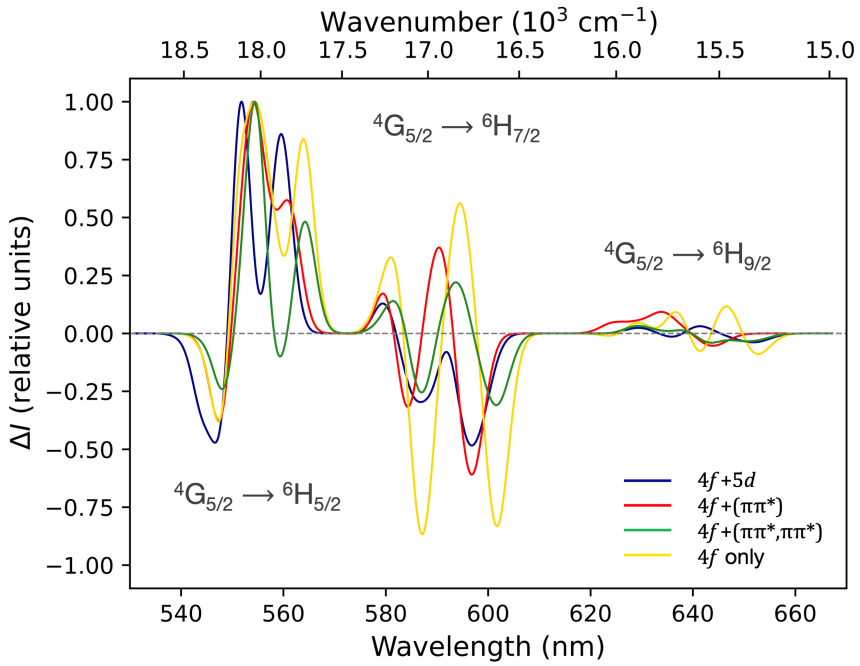

Figure S9 Simulated CPL spectra of $[Sm^{III}(cryptate)]^{3+}$ similar to Figure 4 but with tiny full width at half maximum of 152 cm^{-1} and with all spectra normalised such as the transition at 554 nm is set up to 1.

Table S1 Structural difference between the optimised structures of $[Sm^{III}(cryptate)]^{3+}$ in gas phase and in solvent (methanol), computed at the ZORA-PBE0/TZP DFT level of theory. To assign mentioned atoms, refer to Figure S10, and consider a symmetric assignment between the orange and the green part with a prime superscript for the atoms referring to the green part.

part	features	atoms involved	gas phase	methanol
orange-green	angle (deg.)	H1-Sm-H1'	105.36	107.66
orange	distance (Å)	C1-C2	1.484	1.482
	angle (deg.)	N1-Sm-N2	64.63	64.80
	dihedral angle (deg.)	N1-C1-C2-N2	8.03	6.43
	dihedral angle (deg.)	N2-C3-C4-N3	34.48	34.85
green	distance (Å)	C1'-C2'	1.484	1.482
	angle (deg.)	N1'-Sm-N2'	64.63	64.80
	dihedral angle (deg.)	N1'-C1'-C2'-N2'	8.03	6.43
	dihedral angle (deg.)	N2'-C3'-C4'-N3'	34.48	34.86
grey	dihedral angle (deg.)	N4-C5-C6-N5	49.31	50.70
	dihedral angle (deg.)	O1-C7-C8-O2	51.64	54.83
	dihedral angle (deg.)	C9-C7-C8-C10	70.14	67.13

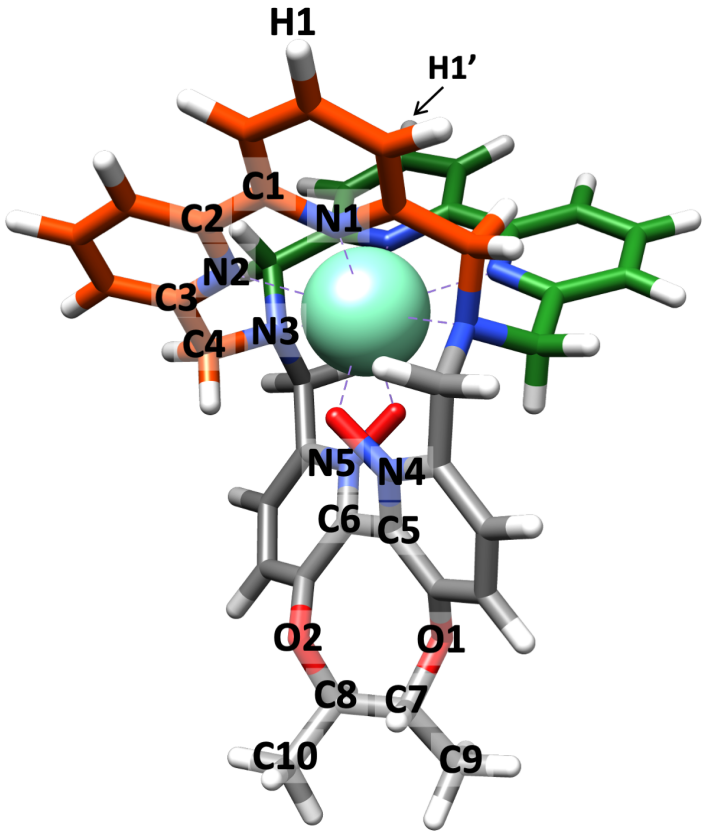

Figure S10 Structure of the $[Sm^{III}(cryptate)]^{3+}$ complex obtained from DFT structural optimization, computed at ZORA-PBE0/TZP in gas phase. The ligand has been divided into three parts for which carbon atoms are coloured in orange, green or grey. Otherwise, the color code is sea-green, Sm; red, O; blue, N; white, H.

Table S2 Calculated energy E, rotatory strength R and oscillator strengths f for $^4G_{5/2} \rightarrow {}^6H_J$ transitions with $J = 5/2, 7/2, 9/2$ at RT from 2' to 0' m_J emissive sublevels. Calculations done at SA-CAS(5,7)SCF/RASSI-SO level of theory for two optimised structures of $[Sm^{III}(cryptate)]^{3+}$ either in methanol or in gas phase.

		in MeOH				in gas			
transition		E (cm^{-1})	R (cgs)	f_{ED}	f_{MD}	E (cm^{-1})	R (cgs)	f_{ED}	f_{MD}
$^4G_{5/2} \rightarrow {}^6H_{5/2}$	2'	21725	-1.52e-44	1.88e-09	2.11e-09	21800	-8.26e-45	1.30e-09	1.03e-09
		21915	-9.99e-44	1.96e-09	9.40e-10	21995	-4.71e-44	1.28e-09	4.63e-10
		22029	-6.62e-45	3.27e-10	1.28e-10	22111	-3.87e-45	2.26e-10	6.81e-11
	1'	21509	-7.35e-45	6.43e-10	1.93e-09	21595	-1.22e-44	4.49e-10	1.00e-09
		21699	2.68e-43	2.59e-09	3.42e-09	21790	1.35e-43	1.65e-09	1.62e-09
		21813	3.66e-44	2.67e-09	5.03e-09	21906	1.68e-44	2.75e-09	2.20e-09
	0'	21422	1.82e-43	3.30e-09	2.75e-09	21489	9.78e-44	1.91e-09	1.27e-09
		21612	-2.69e-44	1.00e-08	5.07e-09	21684	-3.45e-44	9.24e-09	2.54e-09
		21726	1.00e-43	1.87e-09	6.72e-09	21800	6.04e-44	2.06e-09	3.69e-09
$^4G_{5/2} \rightarrow {}^6H_{7/2}$	2'	20612	5.40e-44	4.82e-10	1.51e-09	20685	2.02e-44	2.11e-10	7.57e-10
		20717	-9.54e-44	2.35e-09	8.61e-10	20800	-3.94e-44	9.97e-10	3.91e-10
		20855	6.78e-44	3.79e-09	2.29e-10	20935	3.25e-44	1.69e-09	1.41e-10
		20950	1.81e-44	3.52e-09	3.52e-10	21026	5.86e-45	1.38e-09	1.65e-10
	1'	20396	-8.20e-44	7.95e-09	1.18e-09	20480	-4.49e-44	3.32e-09	5.64e-10
		20502	1.41e-43	6.60e-09	1.31e-09	20595	6.42e-44	3.54e-09	6.36e-10
		20639	-1.75e-43	7.54e-09	1.76e-09	20730	-5.37e-44	1.82e-09	1.18e-09
		20734	9.25e-46	1.38e-08	4.05e-09	20821	-1.51e-44	6.37e-09	1.52e-09
	0'	20309	-2.32e-43	1.75e-08	5.76e-10	20374	-7.20e-44	6.97e-09	2.31e-10
		20415	1.64e-43	2.08e-08	2.95e-09	20489	3.03e-44	1.05e-08	1.62e-09
		20552	-1.05e-44	1.68e-08	8.16e-09	20624	-2.43e-44	6.87e-09	3.49e-09
		20647	1.93e-44	3.40e-08	3.26e-09	20715	4.45e-44	1.68e-08	2.31e-09
$^4G_{5/2} \rightarrow {}^6H_{9/2}$	2'	19320	1.68e-45	6.70e-10	3.01e-12	19392	9.27e-46	4.47e-10	1.72e-12
		19433	-4.57e-46	1.92e-09	5.88e-12	19518	-6.26e-46	1.04e-09	2.74e-12
		19507	2.43e-45	2.62e-10	1.11e-11	19584	1.04e-45	8.96e-11	5.05e-12
		19588	1.84e-44	1.05e-09	5.15e-11	19662	9.43e-45	6.20e-10	2.66e-11
		19657	-1.86e-45	5.93e-10	5.66e-12	19740	-9.44e-46	3.26e-10	3.77e-12
	1'	19104	-3.29e-44	3.62e-09	3.88e-11	19187	-1.48e-44	1.85e-09	2.07e-11
		19217	-3.23e-44	5.87e-09	3.94e-11	19313	-1.67e-44	3.38e-09	2.15e-11
		19291	1.82e-45	3.00e-09	5.15e-11	19379	3.23e-45	1.67e-09	2.73e-11
		19372	-1.63e-44	6.57e-10	9.04e-11	19457	-6.71e-45	2.59e-10	3.39e-11
		19441	3.30e-45	1.31e-08	5.10e-11	19535	2.56e-45	6.91e-09	2.84e-11
	0'	19017	-1.79e-44	2.82e-09	1.51e-11	19081	-7.85e-45	1.25e-09	8.52e-12
		19130	2.04e-44	2.11e-09	2.85e-11	19207	8.28e-45	7.72e-10	1.84e-11
		19204	6.73e-45	4.58e-09	5.52e-11	19273	1.33e-45	2.51e-09	4.02e-11
		19285	-6.80e-45	6.51e-10	1.26e-10	19351	-1.37e-45	2.59e-10	5.91e-11
		19354	2.40e-44	3.12e-09	3.09e-11	19429	1.00e-44	1.42e-09	1.31e-11

Table S3 Energetic splitting of four spectroscopic levels of $[Sm^{III}(cryptate)]^{3+}$ complex, at SA-RAS[7,1,1,1,7,1]SCF/RASSI-SO level of theory.

Spectroscopic term	Kramres doublets	Energy (cm^{-1})
$^4G_{5/2}$	2'	21 149
	1'	20 956
	0'	20 874
$^6H_{9/2}$	4	2 570
	3	2 462
	2	2 395
	1	2 335
	0	2 275
$^6H_{7/2}$	3	1 333
	2	1 234
	1	1 116
	0	1 042
$^6H_{5/2}$	2	273
	1	103
	0	0

Table S4 Boltzmann population in percentage of the Kramers doublets composing the emissive $^4G_{5/2}$ level at various temperatures for $[Sm^{III}(cryptate)]^{3+}$ complex, at SA-RAS[7,1,1,1,7,1]SCF/RASSI-SO level of theory.

Kramers doublets	0K	60K	120K	180K	240K	298K
2'	0	0	3	7	11	14
1'	0	12	27	32	34	35
0'	100	87	71	61	55	51

Table S5 Calculated energy E, rotatory strength R and oscillator strengths f for $^4G_{5/2} \rightarrow {}^6H_J$ transitions with $J = 5/2, 7/2, 9/2$ at RT from 2' to 0' m_J emissive sublevels. Calculations done at SA-RAS[7,1,1,1,7,1]SCF/RASSI-SO level of theory for $[Sm^{III}(cryptate)]^{3+}$.

transition		E (cm^{-1})	R (cgs)	f_{ED}	f_{MD}
$^4G_{5/2} \rightarrow {}^6H_{5/2}$	2'	20875	-3.52e-44	4.34e-10	2.26e-09
		21045	-1.77e-43	3.54e-09	1.00e-09
		21148	-1.38e-44	6.41e-10	1.32e-10
	1'	20682	8.34e-44	4.51e-09	2.10e-09
		20852	3.58e-43	5.43e-09	3.17e-09
		20955	8.28e-44	1.21e-09	4.56e-09
	0'	20601	2.05e-43	3.87e-09	2.22e-09
		20770	1.30e-43	4.38e-09	4.90e-09
		20874	1.68e-44	2.37e-09	6.70e-09
$^4G_{5/2} \rightarrow {}^6H_{7/2}$	2'	19815	9.05e-44	1.80e-09	1.75e-09
		19914	-1.23e-43	5.04e-09	7.44e-10
		20033	1.19e-43	1.12e-08	3.02e-10
		20106	-1.01e-44	7.61e-09	3.78e-10
	1'	19622	-2.00e-43	1.64e-08	9.21e-10
		19721	2.35e-43	2.28e-08	1.68e-09
		19840	-2.10e-43	1.08e-08	2.27e-09
		19913	-5.72e-44	3.47e-08	3.12e-09
	0'	19540	-3.02e-43	4.27e-08	4.59e-10
		19639	1.24e-43	5.32e-08	2.85e-09
		19758	-5.89e-44	3.25e-08	6.32e-09
		19832	1.62e-43	7.72e-08	4.01e-09
$^4G_{5/2} \rightarrow {}^6H_{9/2}$	2'	18579	1.00e-45	5.91e-09	3.44e-12
		18686	1.99e-45	1.10e-08	5.58e-12
		18753	1.96e-45	1.56e-09	7.79e-12
		18813	2.89e-44	5.44e-09	5.02e-11
		18874	-1.27e-45	1.09e-09	7.11e-12
	1'	18385	-4.87e-44	1.38e-08	3.82e-11
		18493	-5.79e-44	3.58e-08	3.69e-11
		18560	3.80e-44	2.41e-08	4.77e-11
		18620	-4.30e-45	2.25e-09	4.53e-11
		18681	2.55e-44	4.87e-08	4.48e-11
	0'	18304	-2.83e-44	1.15e-08	1.34e-11
		18411	3.87e-44	1.23e-08	2.87e-11
		18478	3.71e-44	2.30e-08	6.30e-11
		18538	4.05e-44	1.62e-08	7.75e-11
		18599	4.96e-45	4.78e-08	1.26e-11

Table S6 Energetic splitting of four spectroscopic levels of $Sm^{III}(hfac)_3(^{i}Pr\text{-}PyBox)$ complex, at SA-CAS(5,7)SCF/RASSI-SO level of theory.

Spectroscopic term	Kramres doublets	Energy (cm^{-1})
$^4G_{5/2}$	2'	22 057
	1'	21 966
	0'	21 871
$^6H_{9/2}$	4	2 568
	3	2 534
	2	2 501
	1	2 403
	0	2 375
$^6H_{7/2}$	3	1 287
	2	1 248
	1	1 172
	0	1 067
$^6H_{5/2}$	2	187
	1	141
	0	0

Table S7 Boltzmann population in percentage of the Kramers doublets composing the emissive $^4G_{5/2}$ level at various temperatures for $Sm^{III}(hfac)_3(^{i}Pr\text{-}PyBox)$ complex, at SA-CAS(5,7)SCF/RASSI-SO level of theory.

Kramers doublets	0K	60K	120K	180K	240K	298K
2'	0	1	8	13	17	20
1'	0	9	22	28	30	31
0'	100	90	70	59	53	49

Table S8 Calculated energy E, rotatory strength R and oscillator strengths f for $^4G_{5/2} \rightarrow {}^6H_J$ transitions with $J = 5/2, 7/2, 9/2$ at RT from 2' to 0' m_J emissive sublevels. Calculations done at SA-CAS(5,7)SCF/RASSI-SO level of theory for $Sm^{III}(hfac)_3(^i$Pr-PyBox).

transition		E (cm^{-1})	R (cgs)	f_{ED}	f_{MD}
$^4G_{5/2} \rightarrow {}^6H_{5/2}$	2'	21869	-6.44e-45	1.10e-10	3.02e-09
		21915	-3.42e-44	1.34e-10	2.25e-09
		22057	-8.21e-45	3.26e-10	1.14e-10
	1'	21778	-2.78e-46	3.56e-10	3.66e-09
		21825	-8.84e-45	7.35e-10	2.63e-09
		21966	-2.25e-44	2.06e-10	2.30e-09
	0'	21683	-1.11e-44	5.62e-10	6.99e-10
		21729	1.20e-43	5.95e-10	3.99e-09
		21870	8.92e-44	1.50e-09	9.67e-09
$^4G_{5/2} \rightarrow {}^6H_{7/2}$	2'	20770	-4.07e-44	4.86e-09	1.86e-09
		20808	2.86e-44	9.51e-09	2.21e-09
		20884	-1.51e-44	1.83e-09	7.09e-10
		20989	1.66e-44	1.22e-08	2.26e-10
	1'	20679	2.27e-44	8.31e-09	2.12e-09
		20717	-6.33e-44	1.12e-08	1.42e-09
		20793	2.74e-43	1.58e-08	2.71e-09
		20898	-1.73e-43	2.09e-08	1.61e-09
	0'	20583	4.41e-44	1.53e-08	6.76e-10
		20622	1.26e-44	9.62e-09	1.32e-09
		20698	-4.21e-43	4.36e-08	3.42e-09
		20803	2.87e-43	1.27e-08	6.86e-09
$^4G_{5/2} \rightarrow {}^6H_{9/2}$	2'	19488	8.12e-46	2.25e-09	1.35e-12
		19523	1.94e-45	2.55e-09	2.07e-12
		19555	6.41e-45	2.31e-09	4.28e-12
		19654	2.99e-45	1.42e-09	4.76e-12
		19681	1.39e-45	3.10e-09	3.40e-12
	1'	19397	4.48e-45	1.75e-09	7.23e-12
		19432	-2.35e-45	8.68e-10	8.62e-12
		19464	1.03e-44	2.66e-09	7.73e-12
		19563	6.84e-45	1.42e-09	1.08e-11
		19590	2.24e-45	5.07e-10	7.25e-12
	0'	19302	-3.05e-44	4.64e-09	2.80e-11
		19337	-1.79e-44	3.62e-09	1.31e-11
		19369	-6.04e-45	7.40e-09	2.40e-11
		19467	-8.63e-45	2.07e-09	6.59e-11
		19495	4.54e-45	2.10e-09	2.11e-11